Iterative time integration for poroelasticity with nonlinear permeability

Robert Altmann, Matthias Deiml

Angaben zur Veröffentlichung / Publication details:

Altmann, Robert, and Matthias Deiml. 2024. "Iterative time integration for poroelasticity with nonlinear permeability." PAMM - Proceedings in Applied Mathematics and Mechanics 24 (4): e202400011. https://doi.org/10.1002/pamm.202400011.

Received: 16 April 2024 | Revised: 9 October 2024 | Accepted: 11 October 2024

DOI: 10.1002/pamm.202400011

RESEARCH ARTICLE

Iterative time integration for poroelasticity with nonlinear permeability

Robert Altmann[1] | **Matthias Deiml**[2]

[1]Institute of Analysis and Numerics, Otto von Guericke University Magdeburg, Magdeburg, Germany

[2]Institute of Mathematics, University of Augsburg, Augsburg, Germany

Correspondence
Matthias Deiml, Institute of Mathematics, University of Augsburg, Universitätsstr. 12a, 86159 Augsburg, Germany.
Email: matthias.deiml@uni-a.de

Funding information
Deutsche Forschungsgemeinschaft, Grant/Award Numbers: 467107679, 455719484

Abstract

In this paper, we consider iterative time stepping schemes for poroelasticity including a nonlinearity in the flow equation. For this, we extend recently introduced schemes, which converge with first- and second-order in the linear case, to the nonlinear setting. In each step of the iteration process, the elastic and flow equations are decoupled, which automatically linearizes the system. Numerical examples prove the efficiency of the iterative schemes.

1 | INTRODUCTION

In this paper, we extend two iterative schemes which were recently introduced for linear poroelasticity [1, 2] to the nonlinear setting. More precisely, we consider Biot's quasi-static equations of poroelasticity [3], where the permeability is allowed to depend on the porosity and, hence, on the divergence of the displacement [4]. Such nonlinear terms appear, for example, in geomechanics [5]. A temporal discretization by the implicit Euler scheme not only yields a large coupled system, which needs to be solved in every time step, but due to the nonlinear permeability it also calls for an additional linearization step. Here, a standard choice is a Picard iteration, which is a particular fixed-point iteration. This approach is used, for example, in refs. [4, 6]. Although one typically only needs a few inner iteration steps, the precise number is not known and depends on the strength of the nonlinearity and the desired error tolerance. Even decoupled approaches such as the popular fixed-stress scheme [7–9] need a linearization. Here, the elastic and flow equations are decoupled but the latter is still nonlinear. The situation is different for approaches where one first solves the elastic equation. This is done, for example, in the semi-explicit scheme introduced in refs. [10, 11]. Here, however, a restriction on the coupling strength pops up, which excludes certain applications.

In this paper, we consider the iterative schemes of first- and second-order introduced in refs. [1, 2] and apply them to the nonlinear setting. They combine the advantages of the semi-explicit (first solving the elastic equation such that no additional linearization is necessary) and the iterative approaches (no restriction on the coupling strength for an appropriate number of inner iterations). After the formulation of the two schemes for the nonlinear poroelasticity equation, we consider a numerical example showing the efficiency of these approaches.

2 | NONLINEAR POROELASTICITY

Within this section, we introduce several poroelasticity models with nonlinear permeability. Moreover, we discuss the spatial discretization, which then leads to a nonlinear differential–algebraic equation.

2.1 | PDE model

Let $\Omega \subseteq \mathbb{R}^d$, $d \in \{2, 3\}$, denote the computational Lipschitz domain and $T > 0$ the considered time horizon. In poroelasticity, we are interested in the displacement $u : [0, T] \times \Omega \to \mathbb{R}^d$ and the pressure $p : [0, T] \times \Omega \to \mathbb{R}$ such that

$$-\nabla \cdot \sigma(u) + \nabla(\alpha p) = f \qquad \text{in } (0, T] \times \Omega, \tag{1a}$$

$$\partial_t \left(\alpha \nabla \cdot u + \frac{1}{M} p \right) - \nabla \cdot \left(\frac{\kappa(\nabla \cdot u)}{\nu} \nabla p \right) = g \qquad \text{in } (0, T] \times \Omega \tag{1b}$$

along with suitable initial and boundary conditions. The right-hand sides f and g model the volumetric load and the fluid source, respectively. Moreover, σ denotes the well-known stress tensor from linear elasticity, that is,

$$\sigma(u) = 2\mu\, \varepsilon(u) + \lambda\, (\nabla \cdot u)\, \mathrm{id}, \qquad \varepsilon(u) = \frac{1}{2} \left(\nabla u + (\nabla u)^T \right)$$

with the Lamé coefficients μ and λ. For more details on the involved constants, namely the fluid–solid coupling coefficient α, the Biot modulus M, and the fluid viscosity ν, we refer to refs. [3, 12]. The permeability κ, on the other hand, is allowed to dependent on the porosity in a nonlinear manner. In order to guarantee the existence of a (unique) solution, we follow ref. [4] and make the following assumptions:

i) κ is Lipschitz continuous and
ii) bounded, that is, there exist positive constants κ_- and κ_+ such that $0 < \kappa_- \leq \kappa \leq \kappa_+ < \infty$.

These assumptions imply, in particular, that the diffusion operator in (1b) defines a continuous and elliptic operator. In the following, we discuss particular models which lead to a unique solution (u, p).

2.2 | Displacement-dependent permeability models

As a first example, we consider the network-inspired permeability as described in ref. [13] with an exponential dependence on the displacement [14, 15] and an artificial lower bound to fulfill the above assumptions. This models a network structure where the likelihood of a channel being "open" depends on the local deformation.

Example 2.1 (Network-inspired permeability). Following [13], we set

$$\kappa(s) := \begin{cases} \kappa_0 \delta, & \rho(s) < \hat{\rho}, \\ \kappa_0 \delta + \kappa_0 \dfrac{\rho(s) - \hat{\rho}}{\rho_0 - \hat{\rho}}, & \rho(s) \geq \hat{\rho} \end{cases}$$

with $\delta > 0$, $\rho_0, \hat{\rho} \in (0, 1)$, $\hat{\rho} < \rho_0$, and the porosity ρ defined through

$$\rho(s) = 1 - (1 - \rho_0)\, e^{-s}.$$

Another well-established model is given by the Kozeny–Carman relation [16, 17].

Example 2.2 (Kozeny–Carman-type permeability). In [4, 18], one considers the permeability

$$\kappa(s) := \begin{cases} \kappa_- := \kappa(c_s), & s < c_s, \\ \kappa_0 \dfrac{\rho^3(s)}{(1-\rho(s))^2}, & c_s \le s \le C_s, \\ \kappa_+ := \kappa(C_s), & s > C_s \end{cases}$$

with initially saturated permeability κ_0 and prescribed bounds c_s, C_s such that

$$\frac{\rho_0}{\rho_0 - 1} < c_s < C_s < 1, \qquad \rho_0 \in (0,1).$$

The porosity ρ is given by

$$\rho(s) = \rho_0 + (1-\rho_0)\, s.$$

Similarly, one may also consider nonlinear versions of thermoelasticity [19]. Here, the displacement is caused by the temperature changes and the heat conductivity is allowed to be nonlinear.

2.3 | Spatial discretization

Before we discuss different strategies on the time discretization, we shortly mention the spatial discretization of the nonlinear poroelastic system (1). For more details on the differential–algebraic structure of the system, we refer to ref. [20]. A suitable spatial discretization, for example, by finite elements [21–23], leads to the following problem: seek $u : [0,T] \to \mathbb{R}^{n_u}$ and $p : [0,T] \to \mathbb{R}^{n_p}$ such that

$$\begin{bmatrix} 0 & 0 \\ \mathbf{D} & \mathbf{C} \end{bmatrix} \begin{bmatrix} \dot{u} \\ \dot{p} \end{bmatrix} = \begin{bmatrix} -\mathbf{A} & \mathbf{D}^T \\ 0 & -\mathbf{B}(u) \end{bmatrix} \begin{bmatrix} u \\ p \end{bmatrix} + \begin{bmatrix} f \\ g \end{bmatrix}. \tag{2}$$

We would like to emphasize that we assume that the discretization already includes the assumed boundary conditions. In particular, we assume that the matrices $\mathbf{A}$, $\mathbf{B}(u)$, and $\mathbf{C}$ are symmetric and positive definite. For $\mathbf{B}(u)$, this corresponds to the assumption that κ is positive. The coupling matrix $\mathbf{D} \in \mathbb{R}^{n_p, n_u}$ is assumed to be of full (row) rank. As initial conditions, we expect

$$u(0) = u^0, \qquad p(0) = p^0$$

to be consistent, meaning that $\mathbf{A}u^0 = f(0) + \mathbf{D}^T p^0$. This condition comes from the first equation of (2).

3 | TIME DISCRETIZATION

As we focus on the time discretization of the poroelastic equations, we take the semi-discrete system (2) as a starting point. For all time integration schemes, we consider an equidistant partition of the time interval $[0,T]$ with constant step size τ. This yields discrete time points $t^n = n\tau$. Moreover, assuming the right-hand sides to be continuous, we set $f^n := f(t^n)$ and $g^n := g(t^n)$.

3.1 | Implicit euler scheme

A direct application of the implicit Euler scheme to (2) yields

$$\begin{bmatrix} \mathbf{A} & -\mathbf{D}^T \\ \mathbf{D} & \mathbf{C} + \tau\mathbf{B}(u^{n+1}) \end{bmatrix} \begin{bmatrix} u^{n+1} \\ p^{n+1} \end{bmatrix} = \begin{bmatrix} 0 & 0 \\ \mathbf{D} & \mathbf{C} \end{bmatrix} \begin{bmatrix} u^n \\ p^n \end{bmatrix} + \begin{bmatrix} f^{n+1} \\ \tau g^{n+1} \end{bmatrix}. \tag{3}$$

Hence, one needs to solve a (large) nonlinear system in each time step. For this, one often applies a simple Picard iteration, compare refs. [4, 6]. This is a fixed point iteration which sets $u_0^{n+1} := u^n$, $p_0^{n+1} := p^n$ and computes

$$\begin{bmatrix} \mathbf{A} & -\mathbf{D}^T \\ \mathbf{D} & \mathbf{C} + \tau \mathbf{B}(u_k^{n+1}) \end{bmatrix} \begin{bmatrix} u_{k+1}^{n+1} \\ p_{k+1}^{n+1} \end{bmatrix} = \begin{bmatrix} 0 & 0 \\ \mathbf{D} & \mathbf{C} \end{bmatrix} \begin{bmatrix} u^n \\ p^n \end{bmatrix} + \begin{bmatrix} f^{n+1} \\ \tau g^{n+1} \end{bmatrix}$$

for $k = 0, 1, \dots$. Here, each step requires the solution of a linear but still large and coupled system. In the following, we consider decoupled methods which include an automatic linearization.

3.2 | Semi-explicit euler scheme

In refs. [10, 11] a semi-explicit approach was introduced, which decouples and linearizes the system at the same time. For this, one considers the system

$$\begin{bmatrix} \mathbf{A} & 0 \\ \mathbf{D} & \mathbf{C} + \tau \mathbf{B}(u^{n+1}) \end{bmatrix} \begin{bmatrix} u^{n+1} \\ p^{n+1} \end{bmatrix} = \begin{bmatrix} 0 & \mathbf{D}^T \\ \mathbf{D} & \mathbf{C} \end{bmatrix} \begin{bmatrix} u^n \\ p^n \end{bmatrix} + \begin{bmatrix} f^{n+1} \\ \tau g^{n+1} \end{bmatrix}.$$

Since the matrix on the left is block triangular, one can first solve for u^{n+1} and insert this into the second equation. Hence, the flow and the elasticity equations are decoupled, which allows remarkable computational speed-ups. Moreover, since u^{n+1} is computed first, $\mathbf{B}(u^{n+1})$ is fixed and the equation for p^{n+1} turns linear.

It was shown in ref. [11] that this approach indeed provides a first-order scheme as long as the two equations are weakly coupled. To be more precise, this means that

$$\frac{C_d^2}{c_a c_c} \leq 1$$

with the constants $C_d := \|\mathbf{D}\|_2$, $c_a := 1/\|\mathbf{A}^{-1}\|_2$, and $c_c := 1/\|\mathbf{C}^{-1}\|_2$. In the particular case of poroelasticity, this assumption can be slightly relaxed. More precisely, it can be formulated in terms of the system parameters, namely

$$\frac{\alpha^2 M}{\mu + \lambda} \leq 1.$$

Although this assumption excludes certain applications, this condition is satisfied for a large number of materials; see ref. [24] for parameter tables in the field of geomechanics. Further note that this condition is independent of the nonlinearity.

3.3 | Iterative scheme of first-order

In order to relax the condition of the coupling, that is, to broaden the field of applications, we consider an inner iteration as introduced in ref. [1] for the linear case and translate it to the nonlinear setting. The scheme is closely connected to the drained split [25] but contains an additional relaxation step. For this, we first introduce the relaxation factor

$$\gamma := \frac{2}{2 + \omega} \qquad \text{with} \quad \omega := \frac{\alpha^2 M}{\mu + \lambda} \leq \frac{C_d^2}{c_a c_c}.$$

Given u^n and p^n as approximations of u and p at time t^n, respectively, we first initialize

$$u_0^{n+1} := u^n, \qquad p_0^{n+1} := p^n.$$

We then solve for $k = 0, \dots, K-1$,

$$\begin{bmatrix} \mathbf{A} & 0 \\ \mathbf{D} & \mathbf{C} + \tau \mathbf{B}(\hat{u}_{k+1}^{n+1}) \end{bmatrix} \begin{bmatrix} \hat{u}_{k+1}^{n+1} \\ \hat{p}_{k+1}^{n+1} \end{bmatrix} = \begin{bmatrix} 0 & \mathbf{D}^T \\ 0 & 0 \end{bmatrix} \begin{bmatrix} u_k^{n+1} \\ p_k^{n+1} \end{bmatrix} + \begin{bmatrix} f^{n+1} \\ \tau g^{n+1} + \mathbf{D}u^n + \mathbf{C}p^n \end{bmatrix}. \tag{4}$$

As for the semi-explicit Euler scheme, the matrix on the left-hand side is block triangular such that the system can be solved sequentially. Next, we consider a damping step of the form

$$u_{k+1}^{n+1} := \hat{u}_{k+1}^{n+1}, \qquad p_{k+1}^{n+1} := \gamma\, \hat{p}_{k+1}^{n+1} + (1-\gamma)\, p_k^{n+1}.$$

This, however, is only performed for $k \leq K-2$, that is, not in the last step. After the last time solving (4), we simply set

$$u^{n+1} := u_K^{n+1} := \hat{u}_K^{n+1}, \qquad p^{n+1} := p_K^{n+1} := \hat{p}_K^{n+1}$$

as the new iterates.

We would like to emphasize that in the linear case there is a known bound on K, which guarantees first-order convergence, namely $\omega^K < (2+\omega)^{K-1}$; see ref. [1]. For the nonlinear case, however, such a bound (and the corresponding convergence analysis) remains an open problem.

3.4 | BDF-2

As a representative of implicit schemes of second-order, we apply BDF-2 to the semi-discrete system (2). Since this is a two-step scheme, we need initial data at times t^0 and t^1. More precisely, we assume given data p^0, u^0 as well as p^1, u^1, satisfying the consistency conditions

$$\mathbf{A}u^0 - \mathbf{D}^T p^0 = f(t^0), \qquad \mathbf{A}u^1 - \mathbf{D}^T p^1 = f(t^1).$$

The resulting scheme reads

$$\begin{bmatrix} \mathbf{A} & \mathbf{D}^T \\ 3\mathbf{D} & 3\mathbf{C} + 2\tau \mathbf{B}(u^{n+2}) \end{bmatrix} \begin{bmatrix} u^{n+2} \\ p^{n+2} \end{bmatrix} = \begin{bmatrix} f^{n+2} \\ 2\tau g^{n+2} + \mathbf{D}(4u^{n+1} - u^n) + \mathbf{C}(4p^{n+1} - p^n) \end{bmatrix}. \tag{5}$$

As for the implicit Euler scheme, we combine this approach with a Picard iteration in order to compute the new iterates.

3.5 | Iterative two-step scheme of second-order

Similarly to the approach of Section 3.3, one can also construct a decoupled second-order scheme of BDF-type. Again, we transfer the scheme introduced for linear poroelasticity in ref. [2] to the nonlinear setting. Since the result is a two-step scheme, we assume initial data p^0, u^0 as well as p^1, u^1, both satisfying the consistency condition mentioned in the previous section.

One step of the decoupled scheme then reads as follows: First, initialize

$$u_0^{n+2} := 2u^{n+1} - u^n, \qquad p_0^{n+2} := 2p^{n+1} - p^n.$$

Second, solve for $k = 0, \dots, K-1$,

$$\begin{bmatrix} \mathbf{A} & 0 \\ 3\mathbf{D} & 3\mathbf{C} + 2\tau \mathbf{B}(\hat{u}_{k+1}^{n+2}) \end{bmatrix} \begin{bmatrix} \hat{u}_{k+1}^{n+2} \\ \hat{p}_{k+1}^{n+2} \end{bmatrix} = \begin{bmatrix} 0 & \mathbf{D}^T \\ 0 & 0 \end{bmatrix} \begin{bmatrix} u_k^{n+2} \\ p_k^{n+2} \end{bmatrix} + \begin{bmatrix} f^{n+2} \\ 2\tau g^{n+2} + \mathbf{D}(4u^{n+1} - u^n) + \mathbf{C}(4p^{n+1} - p^n) \end{bmatrix}, \tag{6}$$

which is again a decoupled system. Except for the last step, that is, for $k \leq K-2$, we then apply the relaxation step as before, that is, we set

$$u_{k+1}^{n+2} := \hat{u}_{k+1}^{n+2}, \qquad p_{k+1}^{n+2} := \gamma\, \hat{p}_{k+1}^{n+2} + (1-\gamma)\, p_k^{n+2}$$

with γ as defined in Section 3.3. Finally, we set

$$u^{n+2} := \hat{u}_K^{n+2}, \qquad p^{n+2} := \hat{p}_K^{n+1}$$

in the last step.

Again, we mention the bound on the iteration number K for the linear case, which reads $3\,\omega^K < (2+\omega)^{K-1}$ according to ref. [2]. For the nonlinear setting, such a bound is still unknown.

4 | NUMERICAL EXAMPLE

For the numerical study of the iterative schemes, we revisit Example 2.1 with the network-inspired permeability. As in ref. [11] we consider $\Omega = (0,1)^2$, $T = 1$, and set the parameters of the nonlinearity to

$$\kappa_0/\nu = 8 \cdot 10^{-10}, \qquad \delta = 0.01, \qquad \rho_0 = 0.4, \qquad \hat{\rho} = 0.2.$$

The remaining material parameters correspond to Boise sandstone; see ref. [24, Section 3.3.4]. In particular, we set

$$\lambda = 7.826 \cdot 10^8, \qquad \mu = 1.826 \cdot 10^9, \qquad \alpha = 0.85, \qquad M = 7 \cdot 10^9,$$

which yields a coupling constant of $\omega = \alpha^2 M/(\mu+\lambda) \approx 1.94$.

The right-hand sides are given by

$$f \equiv 0, \qquad g(x,t) = 30\, \sin(\pi x_1)\, \exp(-t).$$

As initial condition, we set

$$p^0(x) = 50\,(1-x_1)\,x_1\,(1-x_2)\,x_2$$

with its consistent counterpart for u^0.

We compare the schemes introduced in Section 3 for this problem. The calculations were run on two Xeon Platinum 8362 Processors, each having 32 cores of 2.8 GHz. The corresponding reference solution is obtained by the fully implicit BDF-2 with time step size $\tau = 2^{-10}$. For the spatial discretization, we choose the mesh size $h = 2^{-7}$ for the reference as well as the experimental calculations. Hence, we only consider the temporal errors. We then compute approximate solutions using (3), (4), (5), and (6) for time step sizes 2^{-k} with $k = 3, \dots, 7$. For the implicit schemes, we stop the Picard iteration when the residual of the nonlinear equation (3) or (5) falls below 10^{-9}. For the iterative schemes, we use fixed numbers of inner iterations. The first-order scheme (4) converges even for $K = 1$, while the second-order scheme needs at least $K = 2$. To reach a higher accuracy in the nonlinearity, we also test both approaches with $K = 4$ and $K = 7$. The implicit methods use BiCGStab with a Schur-type preconditioner, while the iterative methods use CG for both subsystems with an algebraic multigrid preconditioner [26].

The convergence histories are illustrated in Figure 1. As expected, the schemes (3) and (4) converge with order one, whereas (5) and (6) show second-order convergence (as long as the number of inner iterations K is chosen sufficiently large). Moreover, the implicit schemes have, in general, a higher accuracy for the same step size. For a fairer comparison, we also compare the dependency of the obtained error and the runtime of the algorithm in Figure 2. There one can see that the increased accuracy of the implicit schemes comes at the price of an over proportionally increased runtime. As such, the semi-explicit schemes (4) and (6), at least for the chosen problem, are more efficient for all target accuracies. Surprisingly, the best choice for the number of inner iterations for the first-order scheme (4) seems to be $K = 4$ even though convergence is already observed for $K = 1$. This differs from the findings in the linear case, compare ref. [1].

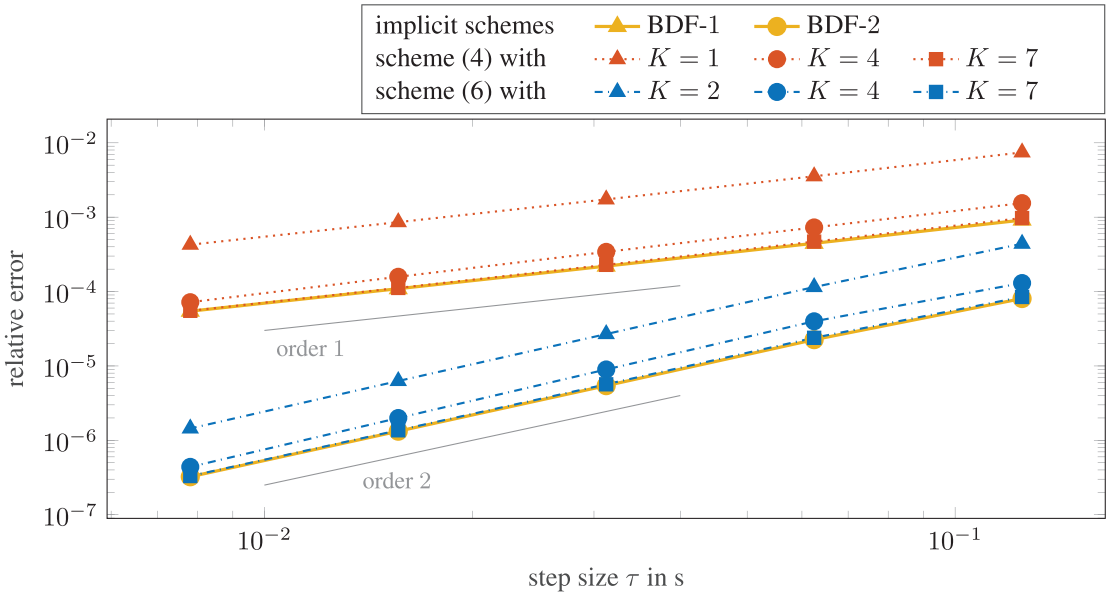

FIGURE 1 Convergence plot the implicit BDF schemes (3) and (5) as well as the iterative schemes (4) and (6). For all calculations we used $h = 2^{-7}$. The reference solution was obtained using the second-order BDF scheme (5) with $\tau = 2^{-10}$. Errors are computed as an L^1 average over the time interval $[0, 1]$ using the Euclidean norm of the finite element vector spaces.

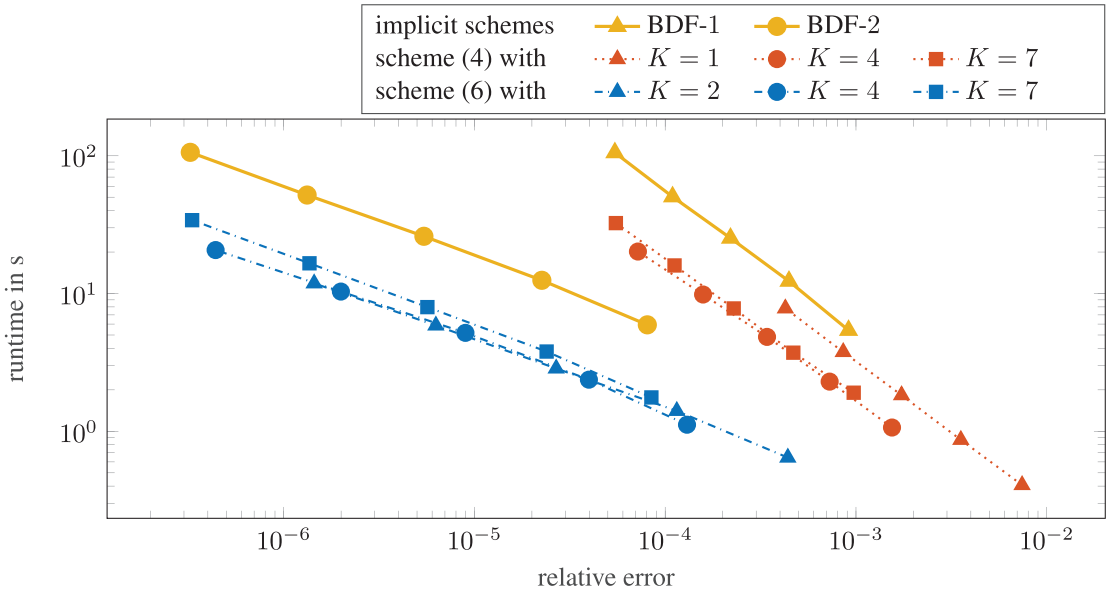

FIGURE 2 Comparison of the runtimes for the four schemes (3)–(6). Errors were computed as in Figure 1. The runtimes for the second-order schemes also include the initialization costs of computing p^1, u^1 using an implicit Euler step.

ACKNOWLEDGMENTS

Both authors acknowledge support by the Deutsche Forschungsgemeinschaft (DFG, German Research Foundation) through the projects 467107679 (RA) and 455719484 (MD), respectively.

Open access funding enabled and organized by Projekt DEAL.

ORCID

Matthias Deiml https://orcid.org/0009-0008-1051-8299

REFERENCES

1. Altmann, R., & Deiml, M. (2024). A novel iterative time integration scheme for linear poroelasticity. *Electronic Transactions on Numerical Analysis*, *60*, 256–275.
2. Altmann, R., & Deiml, M. (2024). A second-order iterative time integration scheme for linear poroelasticity. *ArXiv preprint 2403.12699*.
3. Biot, M. A. (1941). General theory of three-dimensional consolidation. *Journal of Applied Physics*, *12*(2), 155–164.
4. Cao, Y., Chen, S., & Meir, A. J. (2013). Analysis and numerical approximations of equations of nonlinear poroelasticity. *Discrete and Continuous Dynamical Systems - Series B*, *18*(5), 1253–1273.
5. Zoback, M. D. (2010). *Reservoir Geomechanics*. Cambridge University Press.
6. Brown, D. L., & Vasilyeva, M. (2016). A generalized multiscale finite element method for poroelasticity problems II: Nonlinear coupling. *Journal of Computational and Applied Mathematics*, *297*, 132–146.
7. Wheeler, M. F., & Gai, X. (2007). Iteratively coupled mixed and Galerkin finite element methods for poro-elasticity. *Numerical Methods for Partial Differential Equations*, *23*(4), 785–797.
8. Kim, J., Tchelepi, H. A., & Juanes, R. (2011). Stability and convergence of sequential methods for coupled flow and geomechanics: fixed-stress and fixed-strain splits. *Computer Methods in Applied Mechanics and Engineering*, *200*(13-16), 1591–1606.
9. Mikelić, A., & Wheeler, M. F. (2013). Convergence of iterative coupling for coupled flow and geomechanics. *Computational Geosciences*, *17*(3), 455–461.
10. Altmann, R., Maier, R., & Unger, B. (2021). A semi-explicit integration scheme for weakly-coupled poroelasticity with nonlinear permeability. *PAMM*, *20*(1), e202000061.
11. Altmann, R., & Maier, R. (2022). A decoupling and linearizing discretization for poroelasticity with nonlinear permeability. *SIAM Journal of Scientific Computing*, *44*(3), B457–B478.
12. Showalter, R. E. (2000). Diffusion in poro-elastic media. *Journal of Mathematical Analysis and Applications*, *251*(1), 310–340.
13. Rahrah, M., Lopez-Peña, L. A., Vermolen, F., & Meulenbroek, B. (2020). Network-inspired versus Kozeny–Carman based permeability-porosity relations applied to Biot's poroelasticity model. *Journal of Mathematics in Industry*, *10*(19).
14. Lai, W. M., & Mow, V. C. (1980). Drag-induced compression of articular cartilage during a permeation experiment. *Biorheology*, *17*(1-2), 111–123.
15. Holmes, M. H., & Mow, V. C. (1990). The nonlinear characteristics of soft gels and hydrated connective tissues in ultrafiltration. *Journal of Biomechanics*, *23*(11), 1145–1156.
16. Kozeny, J. (1927). Über kapillare Leitung des Wassers im Boden. *Royal Academy of Science, Vienna, Proceedings Class I*, *136*, 271–306.
17. Carman, P. C. (1937). Fluid flow through granular beds. *Transactions of the Institution of Chemical Engineers*, *15*, 150–166.
18. Bociu, L., Guidoboni, G., Sacco, R., & Webster, J. T. (2016). Analysis of nonlinear poro-elastic and poro-visco-elastic models. *Archive for Rational Mechanics and Analysis*, *222*(3), 1445–1519.
19. Biot, M. A. (1956). Thermoelasticity and irreversible thermodynamics. *Journal of Applied Physics*, *27*, 240–253.
20. Altmann, R., Mehrmann, V., & Unger, B. (2021). Port-Hamiltonian formulations of poroelastic network models. *Mathematical and Computer Modelling of Dynamical Systems*, *27*(1), 429–452.
21. Murad, M. A., & Loula, A. F. D. (1992). Improved accuracy in finite element analysis of Biot's consolidation problem. *Computer Methods in Applied Mechanics and Engineering*, *95*(3), 359–382.
22. Phillips, P. J., & Wheeler, M. F. (2007). A coupling of mixed and continuous Galerkin finite element methods for poroelasticity I: the continuous in time case. *Computational Geosciences*, *11*(2), 131–144.
23. Ern, A., & Meunier, S. (2009). A posteriori error analysis of Euler–Galerkin approximations to coupled elliptic-parabolic problems. *ESAIM: Mathematical Modelling and Numerical Analysis*, *43*(2), 353–375.
24. Detournay, E., & Cheng, A. H. D. (1993). Fundamentals of poroelasticity. In: *Analysis and Design Methods* (pp. 113–171). Elsevier.
25. Kim, J., Tchelepi, H. A., & Juanes, R. (2011). Stability and convergence of sequential methods for coupled flow and geomechanics: drained and undrained splits. *Computer Methods in Applied Mechanics and Engineering*, *200*(23-24), 2094–2116.
26. Yang, U. M., & Henson, V. E. (2002). BoomerAMG: A parallel algebraic multigrid solver and preconditioner. *Applied Numerical Mathematics*, *41*(1), 155–177.

How to cite this article: Altmann, R., & Deiml, M. (2024). Iterative time integration for poroelasticity with nonlinear permeability. *Proceedings in Applied Mathematics and Mechanics*, *24*, e202400011. https://doi.org/10.1002/pamm.202400011